كلية الهندسة بشبرا
FACULTY OF ENGINEERING AT SHOUBRA
ERJ
PRINT ISSN 3009-6049
ONLINE ISSN 3009-6022

ENGINEERING RESEARCH JOURNAL (ERJ)
Volume (54),Issue (1)
January 2025, pp:175-182
https://erjsh.journals.ekb.eg

Effect of Heating Element Positions on The Thermal Performance of Brick Tunnel Kiln: An Experimental Approach

Mahmoud Mohamed Ibrahim [1,*], Mamdouh Wafaa Shawky Aldosouky [2], Hassanein Abdelmohsen Refaey [2], Ali Ali Abdelaziz [2], Nabil Shafek [2]

[1] Mechanical department ,Elswedy Academy , Tenth of ramadan city.
[2] Department of Mechanical Engineering, Faculty of Engineering at Shoubra, Benha University, Cairo, Egypt.
**Corresponding author*

E-mail address: mahmoudarafat873@gmail.com , masahkhab_68@yahoo.com, hassanein.refaey@feng.bu.edu.eg, ali.ali@feng.bu.edu.eg, n11264@yahoo.com

Abstract: This work experimentally investigates the effect of the heating element (electric coil) positions on the thermal performance of a brick tunnel kiln. A scale 1:4 test section has been utilized. Nine distinct heater positions were examined in the present experimental work, with Reynolds numbers (Re) ranging from 15,938 to 30,890, and as a result, Nusselt Numbers were found from 186 to 285 on most through all settings (nine settings tested), The thermal performance parameters were found to be dependent on the heater positions in each column in test section. The results revealed that at a maximum Reynolds number for each setting of the heating element, the average Nusselt number reached a maximum improvement of 48.8% for setting 2. The results show that the highest percent increase in the local Nusselt number, as the Reynolds number increased from the lowest value to the highest one in each setting, occurs in the longitudinal direction near the wall, reaching a percent value of about 55.7 and 51.3% for settings 2 and 9, respectively.

1. Introduction

Currently, there is a significant focus on energy supply in many industries, particularly in the manufacturing of refractory bricks. This industry is known for its inefficient energy use, as it only utilizes less than 45% of the total energy input [1]. A multitude of scholars have examined energy use in various businesses. The greenware proceeds to the fire zone, wherever fuel is added to raise the temperature to the necessary sintering point. Subsequently, the heated product is transferred to the cooling zone, where it releases a portion of its thermal energy to the circulating air as it flows in the opposing direction. Figure 1 is a representation figure illustrating the temperature spreading along the tunnel kiln.

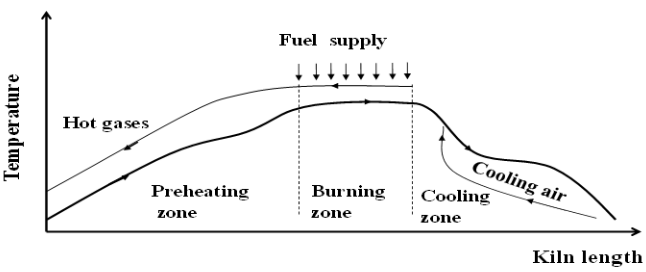

Figure 1: Diagram showing how temperatures change along the tube kiln [1,2].

Due to the high energy utilization in the fire brick business, several researchers have conducted studies on thermal issues inside tunnel kilns [2- 16]. Refaey et al. [2] achieved an experimental investigation on the thermal efficiency of the cooling portion of a tunnel kiln. The study included a broad range of Re, ranging from 11,867 to 25,821, and examined six distinct configurations of brick layouts. The findings indicate that the pressure drop, and convective heat transfer coefficient (h) are significantly influenced by the arrangement pattern. Correlations were derived to estimate the pressure drop and (h) of refractory materials. These correlations were expressed regarding the friction factor and Nu, which depend on the Reynolds number, void number, column spacing to brick thickness, and column spacing to brick length. Refaey et al. [3] investigated two novel approaches using side and U-shaped guiding vanes with different angles. Kiln walls had vanes. Reynolds numbers 13,609–27,634 were tested. Convective heat transmission was considerably modified by settings, guiding vanes, and attack angle. Empirical relationships were also found between Re, attack angle type, brick location, and average Nusselt number.

Vasić et al. [4] used combined thermal analysis and dilatometry to evaluate montmorillonite and hydromica brick clays for construction components. To understand brick clays, plasticity coefficient and drying susceptibility were measured. Pichler et al. [5] presented a model for the anisotropic effective thermal conductivity of bricks utilizing the unit cell model approach. The model addressed conduction and surface-to-surface radiation within the brick material. Four distinct radiation models were introduced, evaluated, and validated through fully resolved computational fluid dynamics simulations across three different brick profiles and experimental setups. A mathematical model by Refaey et al. [6] simulated convection and radiation heat transmission in the vitrified clay pipes kiln. The model used ODEs to depict preheating and firing zone solids and gas temperatures. Stanton numbers above 4 and excess air numbers under 1.7 reduced energy use. Additionally, extra air may control the kiln's thermal process. Al-Hasnawy et al. [7] examined brick tunnel kiln gas circulation with sidewall injection using CFD. A simple design with separate gas flows was mapped between two kiln cars to show wear and ambient temperature variations. The increased vertical distance between opposing air injections increased mixing. When the impulse flow rate was raised to 4 N, the cross-sectional temperature differential fell considerably.

A numerical and mathematical model of ceramic hollow brick drying in an industrial-scale tunnel drier with cross flow was created by Almeida et al. [8]. This research examined product moisture, temperature, relative humidity, and humidity ratio, as well as drying air temperature, relative humidity, and humidity ratio. Data is examined about dryer dry-out time and basis length. Axial velocity and nozzle arrangement were examined in a three-dimensional preheating zone investigation by Refaey and Specht [9]. Their results showed that cross-sectional velocity outweighed axial velocity. Increasing the burner and nozzle radial velocity was necessary to improve heat transmission. Mancuhan et al. [10] constructed a one-dimensional model to explain gas flow, gas-brick heat exchange, and bound water evaporation in a tunnel kiln preheating zone. Two profiles and vent locations were used to introduce surrounding air into the preheating zone. Without ambient air supply, the gas temperature at the preheating zone entry reached 350 °C, which reduced product quality. Gomez et al. [11] analyzed transient heat transport in intermittent ceramic kiln heating and cooling. Kiln pilot tests validated the results. A lot of heat was lost as radiation via the apparatus's side walls.

Refaey et al. [12] studied brick tunnel kiln convective heat transport numerically using CFD. A new brick environment was added. Maximum longitudinal brick rise was 15.3% as brick spacing increased. In summary, most experimental or numerical research focuses on temperature. They also specialize in brick tunnel kiln specialty applications. CFD has advanced as a tool for kiln builders, but understanding the flow field to build a better tunnel kiln takes time. Ngom et al. [13] quantified clay brick transient burning in a typical kiln. They modeled combustion and turbulence using k and Eddy Dissipation. Data showed the goal temperature of 900 °C was met. This led to combustion. The data also showed that the kiln's input had the highest O_2 mass percentage and declined progressively. A recent transient experimental investigation for brick tunnel kilns used guiding vanes as turbulence generators by Refaey et al. [14]. Setting 7 at 135° vane angle yielded a maximum 48% boost in their reported study. All these efforts conserve energy and fossil fuels by regulating tunnel kiln gas flow. Furthermore, A CFD study has been conducted by Refaey et al. [15] to demonstrate the fluid flow characteristics in brick tunnel kiln for four different lattice settings. The flow zones of the vortex generation upstream, downstream, and through the brick column are examined as part of the inquiry. Results showed that at settings 1 and 11, the wall channels had much faster airflow than the column channels. Compared to the other settings, setting 3's vortex creation zone is greater, while setting 1's vortex is much weaker. Cooling the lattice bricks in setting 3 is better than cooling them in the other instances.

The fundamental aim of this experimental study is to suggest altering the location of the heater in various regions of the brick tunnel kiln to enhance heat transmission and observe the resulting pressure decrease. An examination is conducted to study the flow in a modeled test section that is a 1:4 ratio of the real tunnel kiln. Nine brick setting configurations were proposed, built, and evaluated utilizing a suction tunnel kiln. Temperature measurements were conducted on four representative brick models positioned inside center and side wall columns at various orientations. The study investigates the impact of heater position in the longitudinal and transverse positions on heat transfer rate and pressure drop. The analysis includes nine distinct settings, with Re ranging from 15,938 to 30,890. The objective of the current research was to provide kiln engineers with information about the impact of the longitudinal spacing ratio, transversal spacing ratio, Nu with changing Re, and position of heaters.

2. Experimental equipment and process

Figures 2 and 3 displayed a real photo and a schematic representation of the experimental setup, including a centrifugal blower, air duct, and instruments for measuring pressure, velocity, and temperature. A section of a tunnel kiln was replicated at a scale of 1:4, maintaining the same proportions as the original kiln. The present model had dimensions of 0.25 meters in height, 0.35 meters in width, and 2 meters in length. The test area was insulated with glass wool to minimize heat loss to the surrounding environment. There are adjustable glass windows for configuring various brick arrangements at the uppermost part.

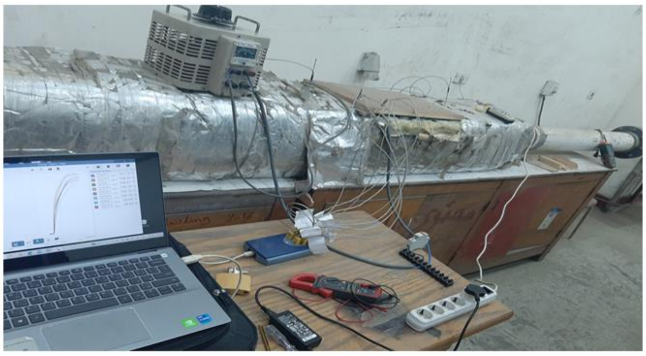

Figure 2: Real photo of the experimental test rig

The tested brick has measurements of 0.114 meters in length, 0.033 meters in width, and 0.058 meters in height. The brick under examination was composed of fire clay to replicate the characteristics of a genuine brick. The arrangement of the setting followed the flow path displayed in Figure 4, which displayed setting 1. The brick arrangement is characterized by columns, rows, and layers. The columns are oriented at a right angle to the direction of flow (the width of the duct), while rows are aligned with the flow direction (the length of the duct). Layers refer to the quantity of bricks stacked vertically, also known as the duct height.

Brick sittings are arranged in counterflow with air direction. Columns, rows, and layers can identify the brick setting. Columns are oriented perpendicular to the flow direction (duct width), whereas rows align with the flow direction (duct length). Layers represent the number of bricks arranged vertically (duct height), as illustrated in Figure 4, which depicts setting 1.

Figure (4) displays the brick-sized instrumented heater. The heaters' surface roughness matches Firebrick's. Each configuration has two heaters in the same flow direction and two transversely. Two thermocouples (type-k) detect the heater's surface temperature, while a digital multimeter measures its voltage and current feed. Air intake and outflow temperatures are recorded via 6 thermocouples. A digital micromanometer (EXTECH HD350) and calibrated Pitot tube assess the air velocity spreading in the test and metering portions, and turbulent flow characteristics determine the average air velocity. The same manometer measures pressure decreases throughout settings.

Refractory bricks were used to make four brick model heating components the same size as the settings. Figure 4 shows the heating brick model construction, brick size, and column spacing. The present work features four vertical brick levels for each scenario. Three rows per test section are perpendicular to the flow. Two flow-oriented columns per test segment. All current arrangements place middle and near wall column longitudinal and transversal heating components in layers. To monitor air intake and outlet temperatures, six K-type thermocouples (2 mm diameter wires) are immediately put into the flow stream at the test section's inlet and exit (three equally separated from the top cover). Eight extra sensors assess the heating brick surface temperature by inserting two K-type thermocouples on each side of each brick model. All thermocouples used in this work are calibrated using a mercury-in-glass thermometer and the accuracy is about ±0.5k. The fifteen-channel data gathering system captured thermocouple temperatures. The static pressure drop between the test section intake and exit is recorded with ±2% accuracy using a Dwyer® series WWDP digital differential pressure transducer and two 2 mm taps on the tunnel bottom surface. Samples of the arrangement options are shown in Figure 5.

2.1 Experimental procedure

Furthermore, Table 1 illustrates the details description of each setting with heater locations. All heaters are in one column. In addition, Table 2 lists the characteristics of the current settings. Between 15,938 and 30,890 Reynolds numbers, all parameters are examined.

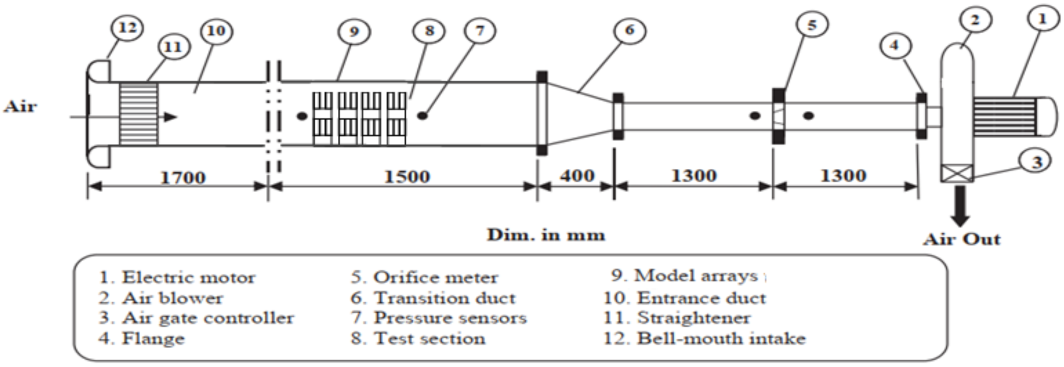

Figure 3: Schematic drawing of the experimental test rig.

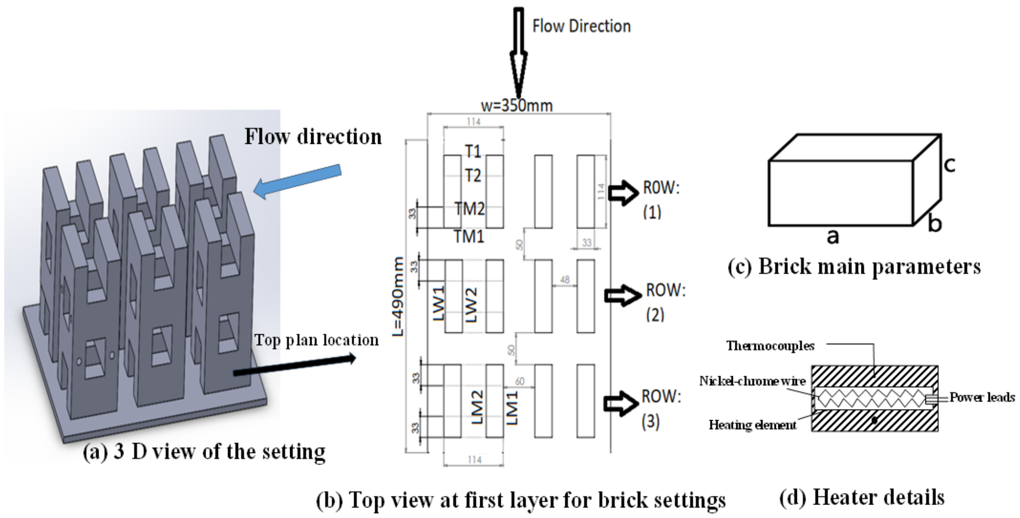

Figure 4: Details of the brick setting.

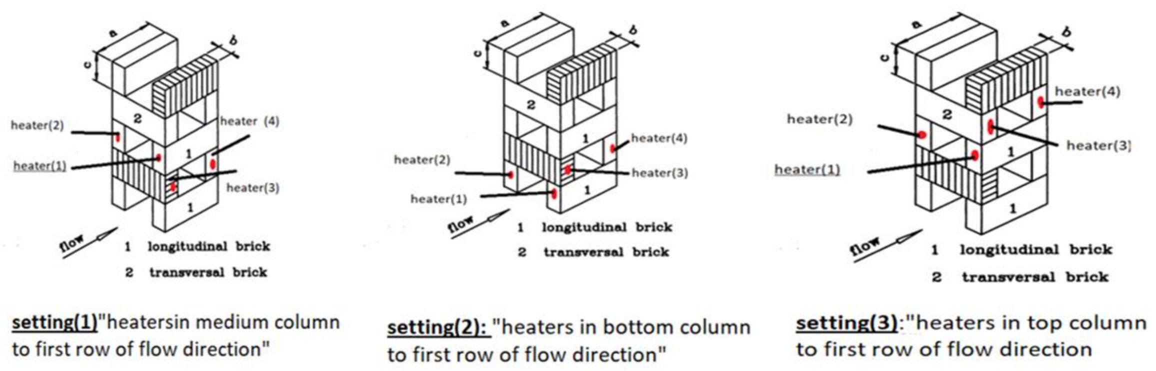

Figure 5: Structure of settings according to heaters' positions in the first column.

Table 1: Heaters positions in each setting.

Setting	Set. (1)		Set. (2)		Set. (3)		Set. (4)		Set. (5)		Set. (6)	
Heaters positions	LW, LM	T, TM	LW, LM	T, TM	LW, LM	T, TM	LW, LM	T, TM	LW, LM	T, TM	LW, LM	T, TM
Row No.	1						2					
Layer No.	3	2	1	2	3	4	3	2	1	2	3	4
Setting	Set. (7)		Set. (8)		Set. (9)							
Heaters positions	LW, LM	T, TM	LW, LM	T, TM	LW, LM	T, TM						
Row No.	3											
Layer No.	3	2	1	2	3	4						

LW: is the longitudinal heater near to wall in the longitudinal airflow direction.
LM: is the longitudinal heater near to the middle of the duct.
T: is the transverse heater directly perpendicular to airflow direction.
TM: is the transverse heater behind the heater T and perpendicular to airflow direction.

Table 2: Descriptions of the nine brick settings to four layers.

Setting	No. of bricks	ε	D_h(Cm)	$A_{w,b}$ (cm^2)	$\frac{A_{w,b}}{A_{w,b1}}$ %	Long bricks%	S (cm)	$\frac{s}{a}$	$\frac{s}{b}$
1	48	0.756	8.52	97.76	100	50	6.2	0.54	1.88

2.2 Data reduction

The experiments begin once the equipment is assembled, as presented in [2 and 3]. The initial stage of collecting system data is placing bricks into the test section and arranging them corresponding to the experimented setting parameters. Air velocity is regulated using the calibrated air gate controller. The voltage regulator also controls heater power. The data collecting system records thermocouple and differential pressure transducer outputs in Excel sheets on a laptop.

A total of 54 experiments were conducted across nine brick configurations. The test operation is conducted under steady-state conditions. Furthermore, the achievement is defined by the attainment of stable fluid inlet and outlet temperatures. The variation in the inlet and outlet temperatures of the air stream remained within 0.1 K for (1 minute) before each measurement was recorded. The elementary measurements in heat transfer computations include the following variables: flow rate, inlet and outlet air temperatures, heating brick surface temperatures, voltage drop (V_i), and the current (I_i) passing via the heaters. The heater power (Q_{input}) is controlled using a 5 kW AC transformer and is determined using the following calculation:

$$Q_{input} = V_i I_i \tag{1}$$

The detailed heat transfer calculations are described in [2 and 3], as follows:

$$h_i = \frac{V_i I_i}{A_b\,(T_{s,i} - T_a)} \tag{2}$$

Where $A_b, T_{s,i}$ and T_a are the brick surface area, the surface temperature at the inlet and air temperature, respectively also, ε is the void fraction and is calculated as:

$$\varepsilon = \frac{V_f}{V_d} \tag{3}$$

Nu, Re, and fraction factor are calculated, respectively, as follows:

$$Nu_i = \frac{h_i D_h}{k} \tag{4}$$

$$Re = \frac{U D_h}{\nu} \tag{5}$$

$$f = \frac{\Delta P D_h}{\frac{1}{2} U^2 L} \tag{6}$$

It is possible to calculate the heat exchange rate amongst bricks and air or combustion products as a function of pumping power (R) for each parameter using the following formula:

$$R = \frac{heat\ transfer\ rate(Q)}{pumping\ power(pp)} = \frac{h_{av}A_{w,b}\Delta T}{u.A_d\Delta P} \tag{7}$$

The uncertainties (ω) in this investigation were determined using Kline and McClintock's root sum square combination of input effects [17]. Additionally, brick and duct dimensions were assumed to be 0.5 mm, and air thermal characteristics were subject to ±0.1% error. Parameter uncertainty is computed. For example, average Nu uncertainty was computed as follows.

$$\frac{\omega_{Nu_{ave}}}{Nu_{ave}} = \pm\sqrt{\left(\frac{\omega_{h_{ave}}}{h_{ave}}\right)^2 + \left(\frac{\omega_{D_h}}{D_h}\right)^2 + \left(\frac{\omega_k}{k}\right)^2} = \pm 1.6\ \% \tag{8}$$

Table 3 illustrates the average uncertainties in the main parameters for all experimental series.

Table 3: Average uncertainties.

Parameter	Uncertainty (ω)
u	±2.5%
U	±2.7%
Re	±3.1%
h_{ave}	±0.69%
ΔP	±3.3%
f	±4.5%
Nu_{ave}	±1.6%
Q	±2.12%

3. Results and discussion

The current experimental setup and measuring instruments were validated by a pilot experiment. All of the parameters, including bricks, column spacing, row spacing, and flow rates, were kept constant throughout the tests conducted on setting 1, as mentioned in [2]. To demonstrate the precision of the experimental apparatus and measurement method, the current testing apparatus has been verified in earlier studies conducted by Refaey et al. [2 and 3].

3.1 Local Nusselt number

Figure 6 depicts the variations in the local Nu at both longitudinal and transverse locations for settings 1, 2, and 3, specifically at the lateral close to the wall and middle position close to the channel between the two columns (middle of the duct). The Reynolds number and the local Nu are visible, and the results indicate that the local Nu increases as the Reynolds number increases in both longitudinal and transverse heaters positions. Additionally, Nu in the longitudinal direction is higher for both the middle and lateral positions compared to the transversal ones. Also, the Nu values exhibit their maximum value in the longitudinal position, surpassing all other places. This is due to the significant air velocity on both faces of the longitudinal bricks linked to the transverse ones. This phenomenon occurs due to the flow velocity passing through apertures in the longitudinal brick faces, resulting in an increased heat transfer inside the faced transverse brick which may demonstrate flow separation and a stagnation zone behind it. From the figure, it is demonstrated that setting 2 has the extreme percentage increase in Nu number with about 55.7 % in the longitudinal position (LW) at Re = 30,807.

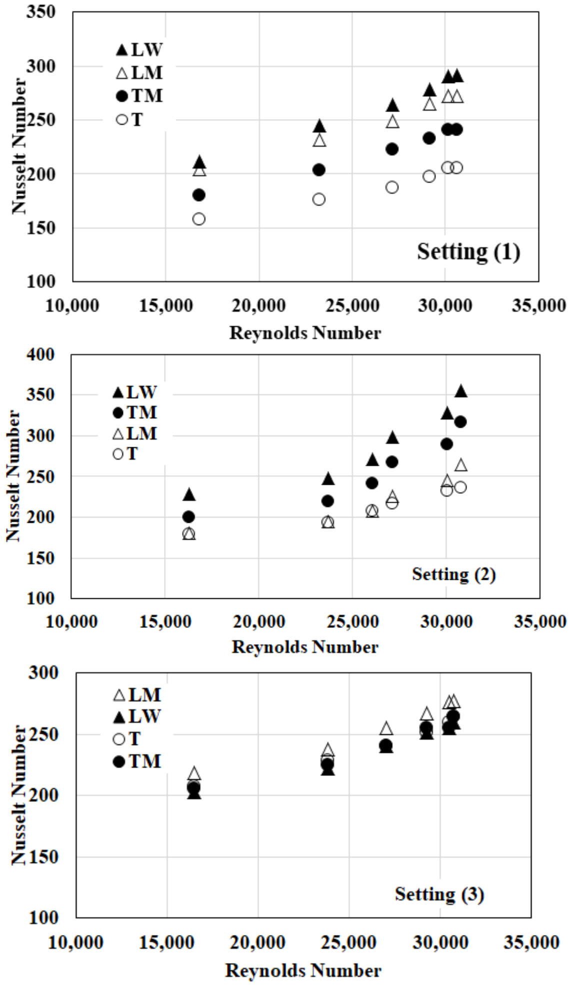

Figure 6: Change of local Nu with Re through first-row at different settings.

Figure 7 displays the variation of the local Nu for transversal and longitudinal bricks at the lateral and middle positions for the second row (settings 4, 5, and 6) as a function of the Re. Setting 4 exhibits the greatest local Nusselt number values in all longitudinal and transversal heaters positions. On the other hand, setting 5 have the lowest values for longitudinal and transversal Nu values compared to all other heaters positions within the given range of Re, as shown in the Figure 7. When compared with the middle one, the wall effect and flow separation are the factors that are responsible for the lowest Nusselt number that was found for both longitudinal and transversal near wall columns.

Figures 6 and 7 show how the Re changes affect the local Nu for both longitudinal and transverse directions for the studied heaters positions. Generally, for all tested conditions, the Nu increases as the Re increases. The data indicates that the local Nu value from the longitudinal heater positions (LW and LM) consistently exceeds the values obtained from other transversal ones. This indicates that heat transfer is more effective at the longitudinal direction which results from turbulent flow on both surfaces, thereby improving heat transfer efficiency.

Transverse bricks, on the other hand, have areas where fluids don't move around freely behind them. This makes heat transfer slower, which is shown by lower Nusselt numbers (Nu). Figure 6 demonstrates that setting 2 yields the highest local Nu values relative to other configurations, indicating that this arrangement is the most effective for heat transfer. In settings 3 and 5 the Nu values for different brick locations (LW, LM, TM, and T) exhibit notable similarity. The findings indicate that the variations in heat transfer among these heater positions are less significant. Given that the local Nu values exhibit minimal variation, settings 3 and 5 may be more appropriate where energy consumption and production are under constraint.

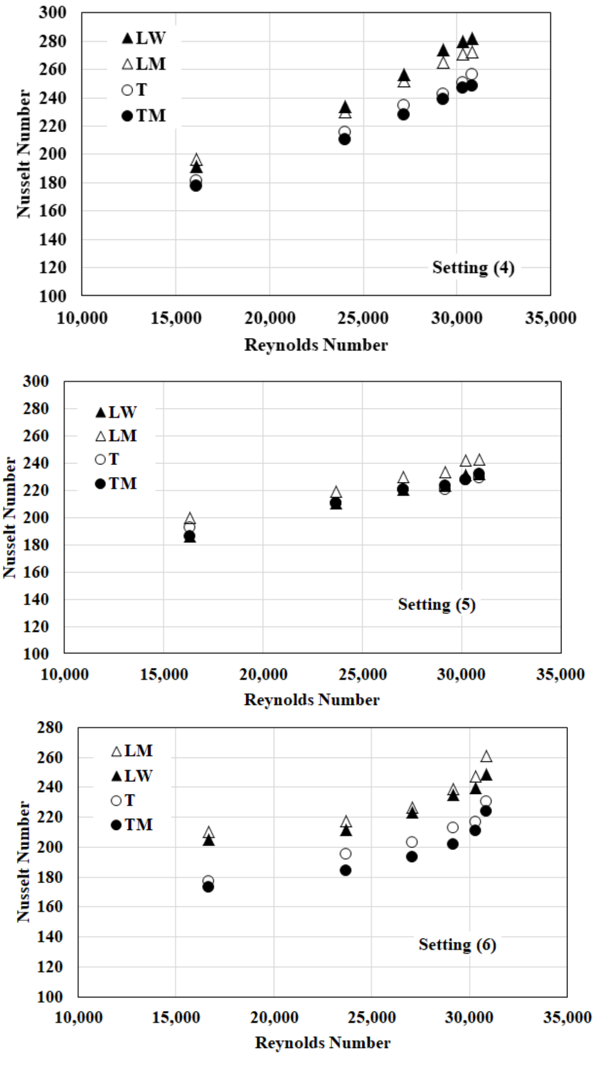

Figure 7: Change of local Nu with Reynolds number through a second row at different settings of heater positions.

3.2 Average Nusselt number

Figure 8 shows the average distributions of Nu vs Re for all settings. Based on these patterns, it is clear that the average Nu follows the same pattern as the local Nu values. Accordingly, the average Nu is lowest in settings 6 and 9 while it is high in setting 7. Due to the intense mixing of fluid in the separated zone and the reduction in boundary layer thickness, the average Nu increases linearly with rising Re, as shown in the picture. In the range of Re from 15,938 to 30,890, the findings demonstrate that the average Nu rises by 48.8 and 41.8 % in setting 2 and 4, respectively as Reynolds number increases from the lower to higher value in each setting. The rise in both flow acceleration and turbulence could explain this.

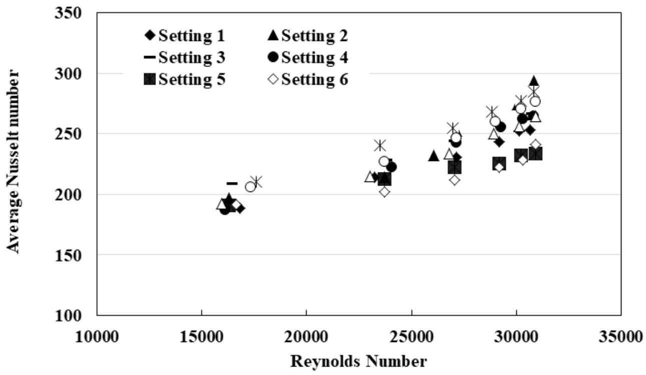

Figure 8: Average Nusselt Number distributions versus Reynolds Number

3.3 Thermal performance

The characteristics of heat transfer are significantly affected by the Reynolds number and other evaluated parameters. However, when considering practical use, it is important to account for the limitation of equal pumping power and to offer the ratio of heat transfer rate to pumping power (R= Qav/PP). The (R) ratio accounts for the pressure decrease over the configuration of bricks. The reduction in pressure across each configuration is essential for enhancing heat transfer. Figure 9 illustrates the effect of the Re on (Qav/PP) in various settings. When considering the pumping power limitation, it is noted that the ratio (Qav) to (PP) has a lower value compared to the case when just the equal mass flow rate restriction is considered. This observation is consistent with the findings shown in Figure 9. Additionally, it has been demonstrated that lower Reynolds numbers have a greater effect on (R) compared to superior values of Re. The influence of the heater position on (Qav/PP) is more pronounced, although the impact of the same settings on (Qav) is not significant within the specified range of Re. The best performance, measured by (Qav/PP), is achieved at settings 9 and 7, with a maximum enhancement of about 18.75, and 15.96 at the lowest Re, respectively. The two settings allow for enhanced airflow and achieve the best heat transfer efficiency at this heater position, while significantly reducing pressure drop. The increase in (R) was lower by at least 1.64 for setting 5. The relationship between the performance ratio and the Re is such that as the Re decreases, the performance ratio rises.

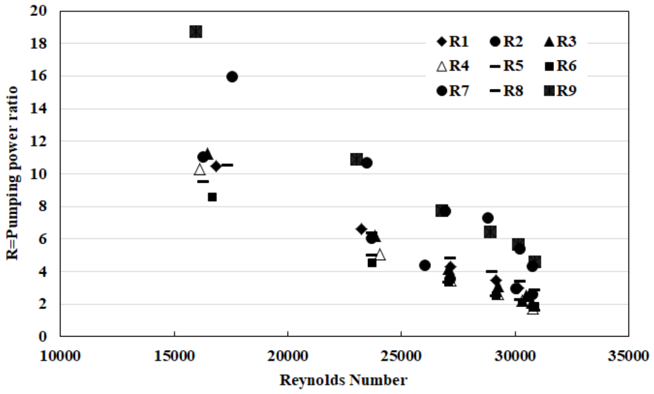

Figure 9: Variations of (R=Qav/PP) against Reynolds number for all settings.

4. Conclusions

This study conducts an experimental analysis to evaluate the impact of heater positioning on the thermal performance of bricks within a tunnel kiln. The local and average Nusselt numbers are analyzed. The main findings of this study are outlined below:

- The local and average Nu is increased with increasing Re for both longitudinal and transverse heater position.
- Setting 4 and 2 largest quantities of local and average Nu for longitudinal and transversal middle bricks.
- The results show that, as the Reynolds number rises, the average Nu rises linearly.
- The results demonstrate that, setting 2 has the extreme percentage increase in Nu number with about 55.7 % in the longitudinal wall position (LW) at Re = 30,641.5.
- Furthermore, setting 2 illustrates the maximum average Nu improves by about 48.8% with an increase of pressure drop by about three times when the tested Re range of 16,301 to 30,807.
- The average heat transfer rate to pumping power ratio(R) is decreased with increasing Re.
- The heat performance, increased by the ratio of average heat transfer rate to pumping power (R), is achieved at setting 9 with 18.75 at Re of 15,937.
- For further work it is recommended to do the study with a higher Reynolds number and with different brick materials with different specifications.

mohamedabada109@gmail.com

REFERENCES

[1] H. A. Refaey, Mathematical Model to Analyze the Heat Transfer in Tunnel Kilns for Burning of Ceramics, Ph.D. dissertation, Otto- von Guericke University, Magdeburg, Germany, (2013).

[2] H.A. Refaey, Ali A. Abdel-Aziz, R.K. Ali, H.E. Abdelrahman, and M.R. Salem, Augmentation of convective heat transfer in the cooling zone of brick tunnel kiln using guide vanes: An experimental study, International Journal of Thermal Sciences, Volume 122, (2017), Pages 172-185.

[3] H.A. Refaey, Ali A. Abdel-Aziz, M.R. Salem, H.E. Abdelrahman, and M.W. Al-Dosoky, Thermal performance augmentation in the cooling zone of brick tunnel kiln with two types of guide vanes, International Journal of Thermal Sciences, Volume 130, 2018, Pages 264-277.

[4] M. V. Vasić, L. Pezo, J. D. Zdravković, Z. Bačkalić, and Z. Radojević, "The study of thermal behavior of montmorillonite and hydromica brick clays in predicting tunnel kiln firing curve," Constr. Build. Mater., vol. 150, pp. 872–879, 2017.

[5] M. Pichler, B. Haddadi, C. Jordan, and M. Harasek, "Modeling the effective thermal conductivity of hollow bricks at high temperatures," Constr. Build. Mater., vol. 309, no. 125066, p. 125066, 2021.

[6] H. A. Refaey, Mohamed A. Karali, Adnan G. Al-Hasnawi, and Eckehard Specht. Mathematical model to simulate the heat transfer in vitrified clay pipes kiln, Conference paper: International Conference on Applied Mechanics and Mechanical Engineering, AMME-18, 03 - 05 April 2018, Military Technical College, Cairo, Egypt.

[7] A. G. T. Al-Hasnawi, H. A. Refaey, T. Redemann, M. Attalla, and E. Specht, and (March 28, 2018). "Computational Fluid Dynamics Simulation of Flow Mixing in Tunnel Kilns by Air Side Injection." ASME. J. Thermal Sci. Eng. Appl. June 2018; 10(3): 031007. https://doi.org/10.1115/1.4038840

[8] G. S. Almeida, J. B. Silva, C. J. Silva, R. Swarnakar, G.A. Neves, and A.G. Lima, Heat and mass transport in an industrial tunnel dryer: Modeling and simulation applied to hollow bricks, Applied Thermal Engineering 55 (2013) 78-86.

[9] H. A. Refaey, and E. Specht, Flow Field Visualization to Simulate the burning of sanitaryware in tunnel Kilns, Proceedings of ICFD11: Eleventh International Conference of Fluid Dynamics December 19-21, 2013, Alexandria, Egypt

[10] S. Kaya, K. Kucukada, and E. Mancuhan, Model-based optimization of heat recovery in the cooling zone of a tunnel kiln, Applied Thermal Engineering 28 (2008) 633–641.

[11] R.S. Gomez, T.R.N. Porto, H.L.F. Magalhães, G. Moreira, A.M.M.C.N. André, R.B.F. Melo, and A.G.B. Lima, Natural Gas Intermittent Kiln for the Ceramic Industry: A Transient Thermal Analysis. Energies 2019, 12, 1568.

[12] H. A. Refaey, M. A. Alharthi, M. R. Salem, A. A. Abdel-Aziz, H.E. Abdelrahman, and M. Karali, Numerical investigations of convective heat transfer for lattice settings in brick Tunnel Kiln: CFD simulation with experimental validation. Therm. Sci. Eng. Prog. 2021, 24, 100934.

[13] M. Ngom, A. Thiam, A. Balhamri, V.Sambou, T. Raffak, and H.A. Refaey, Transient study during clay bricks cooking in the traditional kiln; CFD numerical study. Case Stud. Therm. Eng. 2021, 28, 101672.

[14] H.A. Refaey, B.A.Almohammadi, A.A. Abdel-Aziz, H.E.Abdelrahman, H.A. El-Ghany, M.A.Karali, and M.W.Al-Dosoky, Transient thermal behavior in brick tunnel kiln with guide vanes: Experimental study. Case Stud. Therm. Eng. 2022, 33, 101959.

[15] H.A.Refaey, M.A.Alharthi, A.A.Abdel-Aziz, H.F.Elattar, B.A.Almohammadi, H.E. Abdelrahman, M.A. Karali, E.A.Attia, and M.W. Al-Dosoky, Fluid Flow Characteristics for Four Lattice Settings in Brick Tunnel Kiln: CFD Simulations. Buildings 2023, 13, 733. https://doi.org/10.3390/buildings13030733.

[16] S. J. Kline, F.A. McClintock, Describing uncertainties in single-sample experiments, Mech. Eng. 75(1) (1953) 3–8.

Nomenclature

A	surface area (m^2)
a, b and c	length, thickness, and of brick model
r	radius of holes on the brick
C_p	specific heat capacity of air (J/kgK)
D_h	hydraulic diameter (m)
G	Interstitial mass velocity (kg/m^2s)
h	convection heat transfer coefficient (W/m^2K)
I	current (A)
K	thermal conductivity of air (W/mK)
L	brick setting effective length (m)
$m^{\cdot}$	air mass flow rate (kg/s)

P	pressure (Pa)
pp	pumping power
Q	rate of Heat transfer (W)
R	heat transfer rate to pumping power ratio
T	temperature (°C)
u	air superficial velocity (m/s)
U	air interstitial velocity (m/s)
V	volume (m^3)
V_i	voltage (Volt)
ε	void fraction
ν	kinematic viscosity of air (m^2/s)

Dimensionless groups

f	frictionfactor
Nu	NusseltNumber
Re	Reynolds Number

Subscripts

a	air
av	average
b	bricks
d	duct
f	flow(free)